Magnetic field dependence of the in-plane hole *g* factor in ZnSe- and CdTe-based quantum wells

E. A. Zhukov,[1,2] V. N. Mantsevich,[3,4] D. R. Yakovlev,[1,2] I. S. Krivenko,[5] V. V. Nedelea,[1] D. Kowski,[1] A. Waag,[6] G. Karczewski,[7] T. Wojtowicz,[8] and M. Bayer[1,2]

[1]*Experimentelle Physik 2, Technische Universität Dortmund, 44221 Dortmund, Germany*
[2]*Ioffe Institute, Russian Academy of Sciences, 194021 St. Petersburg, Russia*
[3]*Chair of Semiconductors and Cryoelectronics, Physics Department, Lomonosov Moscow State University, 119991 Moscow, Russia*
[4]*Quantum Technology Center, Physics Department, Lomonosov Moscow State University, 119991 Moscow, Russia*
[5]*I. Institut für Theoretische Physik, Universität Hamburg, 20355 Hamburg, Germany*
[6]*Institute of Semiconductor Technology, Braunschweig Technical University, 38106 Braunschweig, Germany*
[7]*Institute of Physics, Polish Academy of Sciences, PL-02668 Warsaw, Poland*
[8]*International Research Centre MagTop, Institute of Physics, Polish Academy of Sciences, PL-02668 Warsaw, Poland*

(Received 5 January 2021; revised 18 February 2021; accepted 10 March 2021; published 19 March 2021)

The effective *g* factor of holes is measured in modulation-doped ZnSe/(Zn,Mg)(S,Se) quantum wells and from surface-state *p*-doped CdTe/(Cd,Mg)Te quantum wells by time-resolved pump-probe Kerr rotation. The measurements are performed at a temperature of 1.7 K and in magnetic fields up to 5 T applied in the Voigt geometry with orientation perpendicular to the quantum-well growth axis. The absolute value of the in-plane hole *g* factor increases with growing magnetic field in both studied heterostructures. A theoretical model is developed that considers the influence of magnetic field and interface mixing of heavy-hole and light-hole states on the *g* factor. The model results are in good agreement with the experimental data.

DOI: 10.1103/PhysRevB.103.125305

I. INTRODUCTION

One of the main parameters that is associated with the band structure of semiconductors and their nanostructures is the *g* factor (Landé parameter) of electrons and holes. The value and sign of the *g* factors determine the magnetic and magneto-optical properties phenomena in semiconductors, including magnetic resonance, spin relaxation dynamics, the quantum Hall effect, etc. [1–3]. In nanostructures, the quantum confinement reconstructs the electronic bands, which results in a strong change of the *g*-factor values with reducing dimensionality. Although the modification of the electron *g* factor under the influence of external factors (magnetic field, electric field, temperature, intensity of photoexcitation) and internal parameters such as electron concentration was widely studied, both experimentally and theoretically (see Ref. [4] and references therein), the problem of the hole *g*-factor modification is not well investigated and understood. One of the reasons for that is primarily the complexity of *p*-type doping for many compounds. Also, very often the value of the hole *g* factor is much smaller than that for the electrons, and typically the spin relaxation times for holes are much shorter than that for the electrons [5–8]. This provides difficulties for the experimental measurement of hole *g* factors.

Recently, interest in hole spin dynamics has significantly increased. Technological progress in the fabrication of nanostructures (material, dimensionality, doping) and spin engineering with semiconductors offer the possibility to combine materials with different *g* factors to tune the *g*-factor values. The prospects of using the hole spin for quantum information technologies are based on the peculiarities of the hole spin interaction with the lattice nuclei, which is considerably weaker than that for the electrons. The hyperfine interaction between the electron and nuclei spins is the main mechanism for electron spin dephasing and spin relaxation at cryogenic temperatures and small magnetic fields, especially for electrons localized on defects or confined in quantum dots. The hole spin represents an attractive alternative, as the hole hyperfine interaction is much weaker, therefore the hole spin dephasing via nuclear spins is much less efficient. In Ref. [9], a hole spin relaxation time of about 1 ms was determined in (In,Ga)As quantum dots subject to weak magnetic fields. Using time-resolved pump-probe Kerr rotation, spin dephasing times up to 70 ns were measured for localized holes in *p*-type modulation-doped GaAs/$Al_{0.3}Ga_{0.7}As$ quantum wells (QWs) [10], as evaluated from the full width at half-maximum (FWHM) of the resonant spin amplification (RSA) signal at a magnetic field of 0.2 T and temperature of 0.4 K. The hyperfine interaction for holes was measured in *p*-doped InAs/GaAs [11] and (In,Ga)As/GaAs, InP/(Ga,In)P, GaAs/(Al,Ga)As [12,13] quantum dots. It was demonstrated that the hole hyperfine interaction is not negligible and that the hole hyperfine constant has opposite signs for cations and anions and ranges from -15% to $+15\%$ compared to that for electrons.

The hole *g* factor in nanostructures is determined by the peculiarities of the hole energy level spectrum, which in turn is determined by the complex valence band and the interface mixing between the heavy-hole and light-hole states. The mixing is also contributed by strain and quantum

confinement. This problem was investigated theoretically and experimentally in different structures [12,14–22]. Theoretical approaches for the interface mixing between heavy-hole and light-hole states were proposed in Refs. [19,23–29]. In Refs. [23,24], the authors performed an analysis within the envelope-function approximation for the case of oblique incidence of the hole onto the interface, while in Ref. [25] the case of normal incidence on the interfaces grown along directions with rather high Miller indices was considered. In Ref. [26], the mixing for normally incident holes was considered in (001)-grown structures by adding additional terms to the boundary conditions for the hole envelope function at the interfaces. An empirical pseudopotential formalism was used in Ref. [27] to demonstrate numerically that a heavy hole reflected under normal incidence from a single GaAs/AlAs (001) heterojunction contains a considerable light-hole amplitude. A tight-binding model was used to demonstrate the mixing of the heavy-hole and light-hole states for a zero in-plane vector in (001) GaAs-based heterostructures [28]. The generalization of the envelope-function formalism for zinc-blende based (001) interfaces taking into account heavy-hole and light-hole mixing by including off-diagonal terms into the boundary conditions for the envelopes was achieved in Ref. [29].

Available experimental information on the hole g factor in quantum-confined structures is mostly related to the values along the structure growth axis. It was shown that the hole g factor is considerably modified, i.e., its value can change and even its sign can reverse, by increasing the quantum confinement, e.g., by decreasing the QW width or decreasing the quantum dot size. In $GaAs/Al_{0.3}Ga_{0.7}As$ single QWs with decreasing well width from 4.3 nm down to 14 nm, the hole g factors vary from -0.6 to 1.1 for the heavy holes and from 6.5 to 8.6 for the light holes [30]. It was demonstrated in Refs. [6,31,32] that the hole g factor and hole spin dynamics can be tuned by varying an applied gate voltage. Strong magnetic fields can induce additional mixing of the heavy-hole and light-hole states that would result in a modification of the hole g factor. A significant change of the hole g factor from -1.5 down to -0.5 in a 20-nm-thick $CdTe/Cd_{0.65}Mg_{0.35}Te$ quantum well with increasing magnetic field from 6 up to 32 T was reported [33]. In CdSe/CdS colloidal nanoplatelets, the heavy-hole g-factor changes from -0.4 to -0.7 with increasing magnetic fields to 15 T [34]. The in-plane g factor of the heavy hole in the quantum-confined structures, where the heavy-hole and light-hole states are split in energy, is very small. It is zero in the ideal case of the absence of the heavy-hole and light-hole mixing, but in real structures it has some finite values due to the presence of mixing. So far its magnetic field dependence has not been studied in detail.

In the present paper, we report an experimental and theoretical study of the magnetic-field-induced modification of the in-plane hole g factor in ZnSe- and CdTe-based QWs. We utilize the pump-probe Kerr rotation technique to measure the Larmor precession frequency of the hole spin precession in magnetic fields of 0.5–5 T for ZnSe-based QWs and 0.4–1.2 T for CdTe-based QWs. We find a considerable modification of the hole g factor by the magnetic field. We analyze theoretically the role of an external magnetic field applied in Voigt geometry and of the interface mixing of heavy and light holes in this modification. Model calculations allow us to reproduce the experimental dependences.

The paper is organized as follows. Section II contains information about the studied samples and details of the experimental technique. The experimental results are presented in Sec. III. In Sec. IV, the model calculations are described and their results are compared with the experimental data. A discussion is given in Sec. V.

II. EXPERIMENTAL DETAILS

We studied two types of II-VI semiconductor QW structures grown by molecular-beam epitaxy (MBE). The first one are $ZnSe/Zn_{0.89}Mg_{0.11}S_{0.18}Se_{0.82}$ structures with a single QW grown on (100)-oriented GaAs substrates. A specially designed deposition of Zn by atomic-layer epitaxy was used for the growth of a 20-nm-thick ZnSe buffer layer on GaAs. The ZnSe QWs were placed between $Zn_{0.89}Mg_{0.11}S_{0.18}Se_{0.82}$ barriers of 100 and 50 nm thickness. In sample no. 1 (zq 1038), the top barrier has a 3-nm-thick layer doped with chlorine donors; this layer is separated by a 10-nm-thick spacer from the 8-nm-thick QW. The relatively close vicinity of the surface to the QW, which, due to charging, can cause band bending, and the rather thick spacer result in specific features of this structure. Despite the nominal n-type modulation doping, in the absence of above-barrier illumination the QW contains resident holes and not resident electrons, as may be expected. This is confirmed by the observation of hole spin precession in pump-probe Kerr rotation experiments described in Ref. [35]. For above-barrier illumination, resident electrons dominate in the QW.

The sample no. 2 (zq 1113) containing a 10.5-nm-thick QW with otherwise identical material composition is p-type doped using a nitrogen RF plasma. In this case, symmetric modulation doping was achieved by uniform doping of the barriers, excluding 3-nm-thick spacer layers next to the QW. The concentration of the two-dimensional hole gas (2DHG) in the QW is about $n_h \geqslant 10^{10}$ cm^{-2}.

Detailed information about samples no. 1 and no. 2 and the typical optical and magneto-optical properties of ZnSe-based QWs can be found in Refs. [35–39].

The second type is a $CdTe/Cd_{0.78}Mg_{0.22}Te$ QW structure with a 20-nm-thick single QW. Sample no. 3 (no. 062907A) was grown by molecular-beam epitaxy on an undoped (100)-oriented GaAs substrate. Its QW contains resident holes being provided by the method of p-type doping from surface states. The details of this method and the physical processes can be found in Refs. [40,41]. A CdTe 4-μm-thick buffer was initially grown on the GaAs substrate, followed by a $Cd_{0.78}Mg_{0.22}Te$ layer with a thickness of 0.7 μm and the single CdTe QW. The top barrier is formed by 17.5-nm-thick $Cd_{0.78}Mg_{0.22}Te$, which provides p-type doping of the QW from surface states. The density of the resident holes in the QW is about $n_h \approx (3-5) \times 10^9$ cm^{-2}. As will be shown below, the presence of the resident holes is confirmed in the Kerr rotation signal through rather slow (as compared to an electron) Larmor precession oscillations and the suppression of this signal by above-barrier illumination.

We use the time-resolved pump-probe Kerr rotation (TRKR) technique to study the coherent carrier spin dynamics

(for details, see Refs. [2,42]). Spin coherence of holes and electrons was generated by circularly polarized pump pulses (duration 1.5 ps, spectral width about 1 meV) emitted by a Ti:sapphire mode-locked laser operating at a repetition frequency of 75.8 MHz (repetition period $T_R = 13.2$ ns). For the blue spectral range required for measuring the ZnSe-based QWs, the laser pulses were frequency doubled by a BBO (beta barium borate) crystal. The pump helicity was modulated between σ^+ and σ^- polarization at 50 kHz frequency using a photoelastic modulator. The pump and probe beams hit the sample about parallel to the QW growth axis (z-axis). External magnetic fields up to 5 T are applied perpendicular to the growth axis, i.e., in the Voigt geometry. We do not study here the effects related to weak in-plain anisotropy of the hole g factor [35], and therefore the magnetic field was applied along the [100] crystal axis. The measurements are performed at a temperature $T = 1.7$ K.

The pump-excited area of the sample is tested by linearly polarized probe pulses in the reflection geometry. The Kerr rotation (KR) angle of the probe pulses is measured as a function of the delay between the pump and probe pulses using a balanced detector connected to a lock-in amplifier. The pump power was tuned in the range $P_{\text{pump}} = 0.3-10\,\text{W/cm}^2$ and the probe power is kept in the range $P_{\text{probe}} = 0.4-0.7\,\text{W/cm}^2$. The spot size of the pump beam at the sample is about 300 μm and the probe beam size is slightly smaller.

Photoluminescence (PL) spectra are measured at $T = 1.7$ K under continuous-wave (cw) laser excitation with 3.06 eV photon energy. The PL spectra are detected with a Si-based charge-coupled-device camera attached to a 0.5 m spectrometer.

III. EXPERIMENTAL RESULTS

A. ZnSe-based QWs

A photoluminescence spectrum of sample no. 1 is shown in Fig. 1(a). The higher-energy line with the maximum at 2.815 eV corresponds to exciton recombination (X), and the low-energy line (2.808 eV) corresponds to recombination of negatively and positively charged excitons-trions (T). For the pump-probe Kerr rotation experiments, we use resonant excitation of the trion states at the central photon energy of $E_{\text{ex}} = 2.809$ eV. A characteristic KR signal with a damped, periodically oscillating amplitude is observed in transverse magnetic fields from 0.5 T up to 5 T [Fig. 1(b)]. Note that two very different Larmor precession frequencies contribute to the KR signal. This is a direct manifestation of the coherent spin precession of both electrons (at small time delay) and holes. The frequency of these oscillations increases with magnetic field, evidencing an increasing Zeeman splitting of electrons and holes.

Fitting of the experimental spin dynamics by the following expression allows us to evaluate the spin dephasing time, T_2^*, of electrons and holes and their Larmor precession frequency in an external magnetic field, ω_L:

$$\Theta_{\text{KR}} = \sum_i \Theta_{0,i} \exp\left(-\frac{t}{T_{2,i}^*}\right) \cos(\omega_{L,i} t), \qquad (1)$$

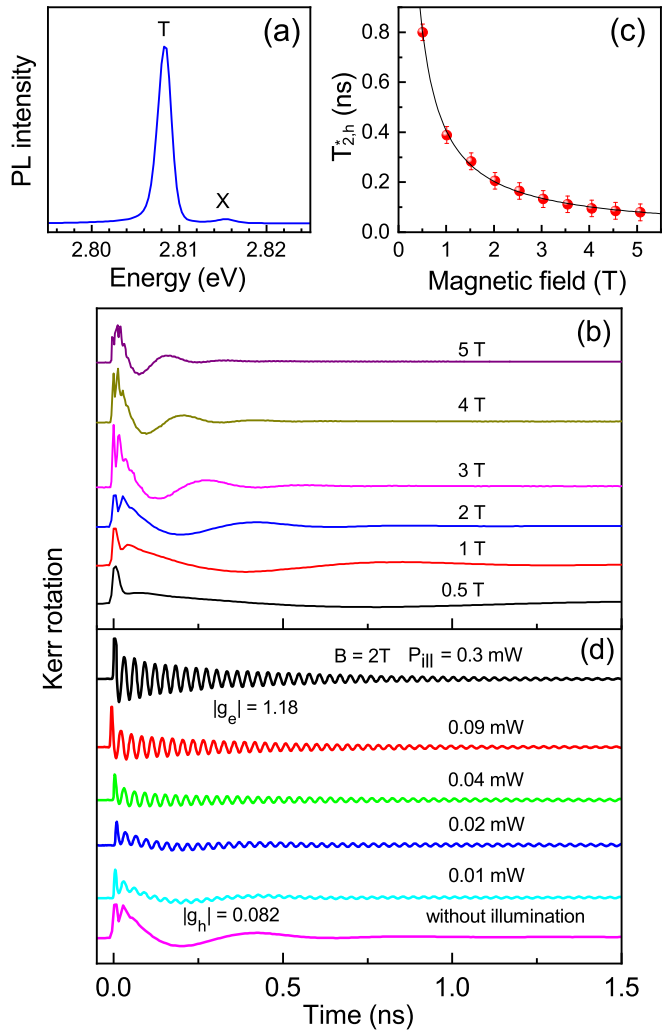

FIG. 1. 8-nm-thick ZnSe/(Zn,Mg)(S,Se) QW (sample no. 1). (a) Photoluminescence spectrum. (b) Pump-probe Kerr rotation signal reflecting the coherent spin dynamics at various magnetic fields, measured at the trion resonance with the laser energy at $E_{\text{ex}} = 2.809$ eV. $P_{\text{pump}} = 1.4\,\text{W/cm}^2$ and $P_{\text{probe}} = 0.4\,\text{W/cm}^2$. (c) Magnetic field dependence of the hole spin dephasing time (circles) and fit with Eq. (3) (line), which gives $\Delta g_h = 0.027$. (d) Kerr rotation traces at the transversal magnetic field of 2 T for different intensities of above-barrier illumination (3.06 eV). All data are at $T = 1.7$ K.

where $\Theta_{0,i}$ is the amplitude of the signal corresponding to the electron and hole components, $i = e, h$. The effective g factor is calculated using the following expression:

$$g_i = \frac{\hbar \omega_{L,i}}{\mu_B B}. \qquad (2)$$

Here $\hbar$ is the Planck constant and μ_B is the Bohr magneton.

One can see in Fig. 1(b) that in low magnetic fields, the small Larmor precession frequency signal is long-living and can be detected for time delays exceeding 1 ns, which is considerably longer than the trion recombination time of about 100 ps. The Larmor precession frequency of this slow precessing component at $B = 0.5$ T corresponds to a g-factor value of 0.078, which is typical for the small values of the in-plane g factor of heavy holes in QWs. Therefore, we assign

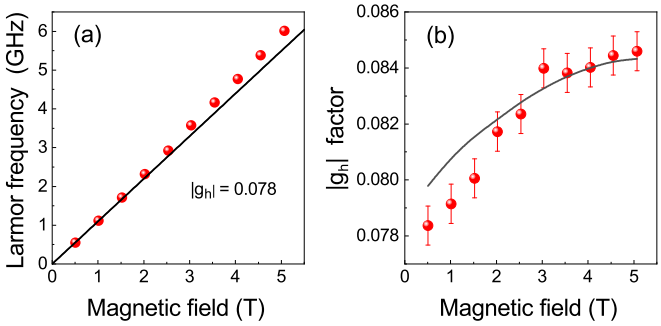

FIG. 2. 8-nm-thick ZnSe/(Zn,Mg)(S,Se) QW (sample no. 1). (a) Magnetic field dependence of the hole Larmor precession frequency (circles) in comparison to linear dependence (black line) assuming $|g_h| = 0.078$. (b) Magnetic field dependence of in-plane $|g_h|$ evaluated from the measured Larmor frequency (red circles) and calculated $|g_h|$ (black line) (See Sec. IV B). $E_{ex} = 2.809$ eV, $P_{pump} = 1.4\,W/cm^2$, $P_{probe} = 0.4\,W/cm^2$, and $T = 1.7$ K.

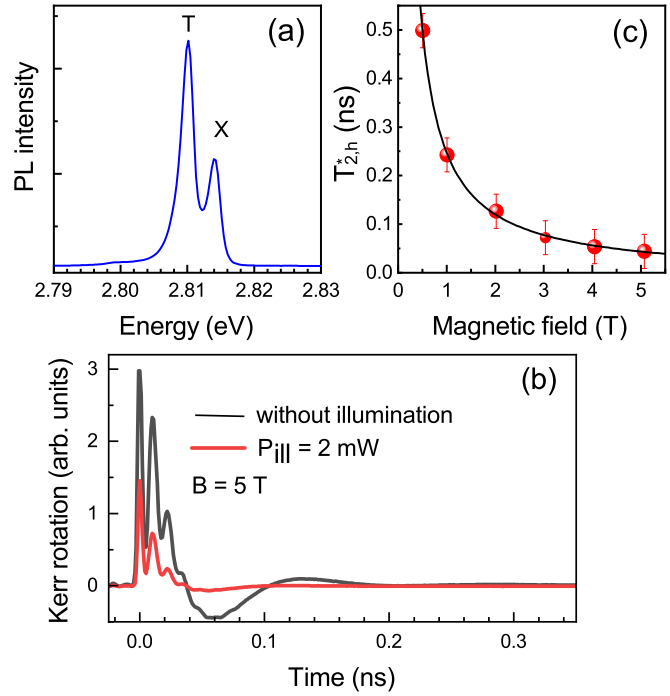

FIG. 3. 10.5-nm-thick ZnSe/(Zn,Mg)(S,Se) QW (sample no. 2). (a) Photoluminescence spectrum. (b) Kerr rotation traces at $B = 5$ T without (black line) and with above-barrier illumination (3.06 eV, $P_{ill} = 2$ mW). $E_{ex} = 2.8145$ eV, $P_{pump} = 1.4\,W/cm^2$, $P_{probe} = 0.4\,W/cm^2$, $T = 1.7$ K. (c) Magnetic field dependence of the hole spin dephasing time (red circles) and fit to the data using Eq. (3) (black line) with $\Delta g_h = 0.045$.

this component to the heavy holes. Note that in bulk ZnSe the value of the hole g factor is 0.28 [43]. The hole spin dephasing time at $B = 0.5$ T is as long as $T^*_{2,h} = 0.8$ ns, but it shortens strongly down to 80 ps at $B = 5$ T; see Fig. 1(c). This strong dependence arises from the spread of the hole g factor, Δg_h. The latter can be evaluated from the fit of the data with the following expression [44,45]:

$$T_2^* = \hbar/\sqrt{(\Delta g \mu_B B)^2 + (g \mu_B \Delta B)^2}, \qquad (3)$$

where ΔB is nuclear field fluctuations, $\hbar$ is the Planck constant, and μ_B is the Bohr magneton. The fit, which is shown by a black line in Fig. 1(c), gives $\Delta g_h = 0.027$. At short delays also a fast oscillation is seen, corresponding to electron spin precession (see below), disappearing on a 100 ps timescale.

The KR signal is strongly modified for above-barrier illumination; see Fig. 1(d). We demonstrate this for $B = 2$ T, where without illumination the signal is dominated by the contribution of resident holes with $|g_h| = 0.082$. With illumination, an electron signal with fast Larmor precession corresponding to $|g_e| = 1.18$ appears, in good agreement with the typical g_e values in ZnSe QWs [35,39]. Note that in bulk ZnSe and QWs, $g_e > 0$. With increasing illumination intensity, the amplitude of the hole contribution decreases and vanishes for illumination powers exceeding 0.32 mW, while the amplitude of the electron contribution increases. This shows that the type of resident carriers in the QWs is changed from holes to electrons, which is a well-established effect for QWs [34] and in particular for ZnSe-based QWs [35,39]. The responsible mechanism is the higher electron mobility in the barrier layers compared to the hole mobility. As a result, the photoexcited electrons are collected in the QW, while the holes tend to become localized in the barriers.

The experimental data on the magnetic field dependence of the hole Larmor precession frequency are shown in Fig. 2(a) by the circles. The black line shows a linear dependence assuming $|g_h| = 0.078$, which corresponds to the value at $B = 0.5$ T. At stronger fields, the measured values deviate considerably from this linear dependence. This means that the in-plane g_h values change with magnetic field. This dependence is shown in Fig. 2(b). $|g_h|$ increases from 0.078 at $B = 0.5$ T up to 0.084 for $B > 3$ T.

The photoluminescence spectrum of sample no. 2 is shown in Fig. 3(a). Similar to sample no. 1, the emission shows two lines at 2.810 eV (trion) and 2.815 eV (exciton).

The spin dynamics for excitation of the exciton ($E_{ex} = 2.8145$ eV) without (black line) and with (red line) above-barrier illumination are shown in Fig. 3(b). The KR signal has two components at $B = 5$ T: a rapidly oscillating one (electron spin precession with $|g_e| = 1.13$) and a slowly oscillating one (hole spin precession with $|g_h| = 0.094$). Both components have about the same amplitude without illumination, but the electron component has the shorter dephasing time. The above-barrier illumination results in suppression of the hole component, similar to the sample no. 1 properties shown in Fig. 1(d).

The magnetic field dependence of $T^*_{2,h}$ is shown in Fig. 3(c). The spin dephasing time reduces from 500 ps at $B = 0.5$ T down to 45 ps at 5 T. The fit of the data with Eq. (3) gives $\Delta g_h = 0.045$.

The magnetic field dependence of the hole Larmor precession frequency is shown in Fig. 4(a). The line is a linear fit to the data with $|g_h| = 0.085$, derived from the data at $B = 1$ T. Similar to sample no. 1, in sample no. 2 the hole g factor depends on the magnetic field, which is seen from the deviation of the experimental data from the linear dependence

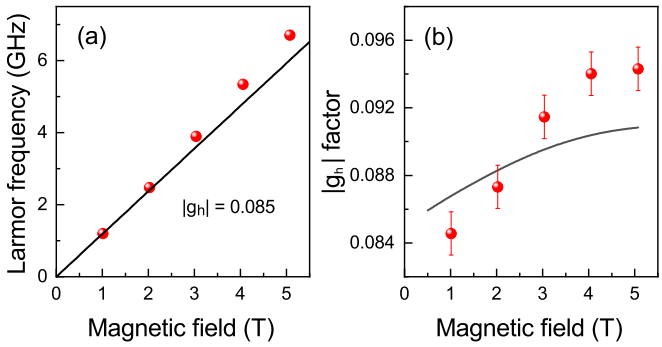

FIG. 4. 10.5-nm-thick ZnSe/(Zn,Mg)(S,Se) QW (sample no. 2). (a) Magnetic field dependence of the hole Larmor precession frequency in comparison to a linear dependence (black line) with $|g_h| = 0.085$. (b) Magnetic field dependence of in-plane $|g_h|$ extracted from measured Larmor frequencies: experimental data (red circles) and calculated $|g_h|$ (black line); for details, see Sec. IV B). $E_{ex} = 2.8145$ eV, $P_{pump} = 1.4\,\mathrm{W/cm^2}$, $P_{probe} = 0.4\,\mathrm{W/cm^2}$, and $T = 1.7$ K.

in Fig. 4(a) and also in Fig. 4(b). $|g_h|$ increases up to 0.094 at $B = 5$ T.

B. CdTe-based QWs

A photoluminescence spectrum of the 20-nm-thick $CdTe/Cd_{0.78}Mg_{0.22}Te$ QW (sample no. 3) is shown in Fig. 5(a). The strongest line at 1.594 eV corresponds to the emission of neutral excitons, and the weaker line at 1.590 eV corresponds to charged excitons, both of negative and positive sign.

Note that *p*-type doping of a QW through surface states is not a very controllable approach. It results in the coexistence of regions with resident holes and resident electrons within the same QW, which are separated in space laterally in the QW plane. As a result, in the TRKR experiments the spin dynamics is contributed by both holes and electrons. A typical signal detected at 1.597 eV is presented in Fig. 5(b) by the black line. It has a complicated shape, and its fitting with Eq. (1) reveals one hole component with $|g_h| = 0.058$ (red line) and three electron components with $|g_{e1}| = 1.604$ (blue line), $|g_{e2}| = 1.483$ (magenta line), and $|g_{e3}| = 1.610$ (green line). The associated spin dephasing times are given in Fig. 5(c). In this sample, the spin dephasing time for the holes ($T_{2,h}^*$) is considerably shorter than that for the electrons. $T_{2,h}^*$ decreases with growing magnetic field strength from $T_{2,h}^* = 0.34$ ns at $B = 0.4$ T down to 0.1 ns at 1.23 T. A fit of $T_{2,h}^*(B)$ dependence using Eq. (3) [red line in Fig. 5(c)] gives $\Delta g_h = 0.076$.

The magnetic field dependence of in-plane $|g_h|$ is shown in Fig. 6. With increasing magnetic field, $|g_h|$ increases from 0.059 at $B = 0.4$ T up to 0.087 at 1.23 T.

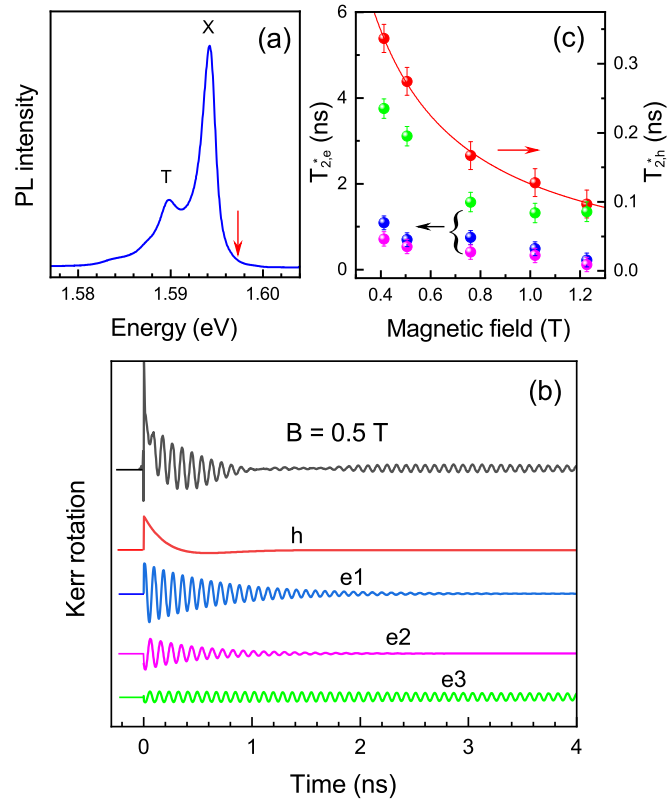

FIG. 5. 20-nm-thick $CdTe/Cd_{0.78}Mg_{0.22}Te$ QW (sample no. 3). (a) Photoluminescence spectrum excited at 1.670 eV. The red arrow marks the energy of the TRKR measurements. (b) Kerr rotation signal measured at $B = 0.5$ T (black line) and its components obtained from decomposition (vertically shifted for clarity): hole (red lines) and electron (blue, magenta and green lines) components. (c) Magnetic field dependence of the spin dephasing time for electrons (blue, magenta and green symbols) and holes (red symbols) and fit to the hole data using Eq. (3) (red line). $P_{pump} = 4.2\,\mathrm{W/cm^2}$, $P_{probe} = 0.7\,\mathrm{W/cm^2}$, $E_{ex} = 1.597$ eV, and $T = 1.7$ K.

IV. MODEL CALCULATIONS OF HOLE *g* FACTORS

A. Effective Hamiltonian

Our theoretical approach for modeling the modification of the measured Landé factors of the holes is based on the envelope-function theory [46]. It takes into account both interface [29] and magnetic-field-induced mixing of the heavy-hole and light-hole states in ZnSe- or CdTe-based QWs. The interface mixing of heavy-hole and light-hole states causes a modification of the Landé factors of holes in comparison with the situation when only a magnetic-field-induced mixing is considered.

The energy spectrum of the valence-band states in bulk semiconductors in the absence of a magnetic field can be approximately described by the four-band Luttinger Hamiltonian [3]:

$$\hat{H}_L = \begin{pmatrix} F & H & I & 0 \\ H^* & G & 0 & I \\ I^* & 0 & G & -H \\ 0 & I^* & -H^* & F \end{pmatrix} \tag{4}$$

with the matrix elements F, G, H, and I equal to

$$F = \varepsilon - \frac{\hbar^2}{2m_0}(\gamma_1 - 2\gamma_2)k_z^2 - \frac{\hbar^2}{2m_0}(\gamma_1 + \gamma_2)\left(k_x^2 + k_y^2\right),$$

$$G = \varepsilon - \frac{\hbar^2}{2m_0}(\gamma_1 + 2\gamma_2)k_z^2 - \frac{\hbar^2}{2m_0}(\gamma_1 - \gamma_2)\left(k_x^2 + k_y^2\right),$$

$$H = \frac{\hbar^2}{m_0}\sqrt{3}\gamma_3 k_z (k_x - ik_y),$$
$$I = \frac{\hbar^2}{2m_0}\sqrt{3}\left[\gamma_2\left(k_x^2 - k_y^2\right) - 2i\gamma_3 k_x k_y\right]. \quad (5)$$

The Hamiltonian is written in the basis of the total angular momentum eigenstates $|J, m_J\rangle$ of the holes with $J = 3/2$ and $m_J = \{3/2, 1/2, -1/2, -3/2\}$. The heavy-hole bands correspond to $m_J = \pm 3/2$ and the light-hole bands to $m_J = \pm 1/2$. ε is the energy of the top of the valence band, located at the Γ-point in the studied materials. k_α are components of the wave vector $\mathbf{k}$ of the holes, m_0 is the free-electron mass, and γ_i $(i = 1, 2, 3)$ are the Luttinger parameters, whose values for ZnSe and CdTe can be found in Refs. [43,47].

For the envelope-function calculations, we place the origin of the coordinate system at the center of the QW and let the z-axis point along the growth direction [001]. One has to replace k_z with its operator form $-i\frac{\partial}{\partial z}$ to derive the effective Hamiltonian of the envelope-function theory from Eq. (4). The Luttinger parameters are assumed to be the same across all heterostructure layers, while the band-edge energy changes in a steplike manner (abrupt interface approximation),

$$\varepsilon(z) = \begin{cases} \varepsilon_{\text{in}}, & |z| \leqslant L/2, \\ \varepsilon_{\text{out}} & \text{otherwise}, \end{cases} \quad (6)$$

where L is the QW width, and ε_{in} and ε_{out} are the energies of the top of the valence band inside and outside the QW, respectively. The edge energies satisfy $|\varepsilon_{\text{out}}| > |\varepsilon_{\text{in}}|$, as is necessary for the existence of discrete hole levels localized in the QW.

Accounting for the external magnetic field has two effects on the effective Hamiltonian. First, it results in the appearance of an extra term describing the action of the field on the Bloch functions—the Zeeman Hamiltonian [48],

$$\hat{H}_Z = -2\mu_B \kappa \mathbf{B}\cdot\mathbf{J} = -\kappa\mu_B \begin{pmatrix} 3B_z & \sqrt{3}B_- & 0 & 0 \\ \sqrt{3}B_+ & B_z & 2B_- & 0 \\ 0 & 2B_+ & -B_z & \sqrt{3}B_- \\ 0 & 0 & \sqrt{3}B_+ & -3B_z \end{pmatrix}. \quad (7)$$

Here, μ_B is the Bohr magneton, $\mathbf{B}$ is the magnetic field vector, $B_\pm = B_x \pm iB_y$, and κ is the magnetic Luttinger parameter [49]. The parameter κ can be either measured in a bulk semiconductor or estimated as $(2\gamma_2 + 3\gamma_3 - \gamma_1 - 2)/3$ [50]. We neglect the small cubic contributions to the $\mathbf{J}$ terms that are responsible for the anisotropic Zeeman splitting. For our specific choice of $\mathbf{B} = (B, 0, 0)$—the magnetic field is applied in the Voigt geometry—the Zeeman term reads

$$\hat{H}_Z = -\kappa\mu_B \begin{pmatrix} 0 & \sqrt{3}B & 0 & 0 \\ \sqrt{3}B & 0 & 2B & 0 \\ 0 & 2B & 0 & \sqrt{3}B \\ 0 & 0 & \sqrt{3}B & 0 \end{pmatrix}. \quad (8)$$

Second, in addition to the Zeeman Hamiltonian, extra terms arise from $\hat{H}_L$. These terms come from redefining the canonical momentum operator, $\mathbf{k} \mapsto \mathbf{k} - (|e|/c\hbar)\mathbf{A}$, where $\mathbf{B} = \nabla \times \mathbf{A}$ [19]. We choose the Landau gauge for the vector potential, $\mathbf{A} = (0, -Bz, 0)$. Since $\mathbf{A}$ depends only on z, we can formulate the envelope-function theory in the usual way, with the envelopes $\chi(z)$ varying only along the growth axis. Assuming normal incidence of the holes with respect to heterostructure interfaces ($k_x = k_y = 0$) and disregarding the small "diamagnetic terms" proportional to $\mathbf{A}^2$, we get the following "shifted" matrix elements of the Luttinger Hamiltonian:

$$F = \varepsilon(z) + \frac{\hbar^2}{2m_{\text{hh}}}\frac{\partial^2}{\partial z^2},$$
$$G = \varepsilon(z) + \frac{\hbar^2}{2m_{\text{lh}}}\frac{\partial^2}{\partial z^2},$$
$$H = -i\sqrt{3}\gamma_3\hbar\omega_c\left\{z, -i\frac{\partial}{\partial z}\right\}_s, \quad (9)$$
$$I = 0,$$

where $m_{\text{hh}} = m_0/(\gamma_1 - 2\gamma_2)$ and $m_{\text{lh}} = m_0/(\gamma_1 + 2\gamma_2)$ are effective masses of the heavy and light holes along the z direction, respectively, and $\omega_c = eB/(m_0 c)$ is the cyclotron frequency. H is proportional to the product of the noncommuting operators z and $-i\frac{\partial}{\partial z}$ that has to be symmetrized in order to ensure hermiticity of the Hamiltonian. Note that we use the common symmetrization rule $\{\hat{A}, \hat{B}\}_s = \frac{1}{2}(\hat{A}\hat{B} + \hat{B}\hat{A})$.

An important effect contributing to the renormalization of the hole g factor is the so called interface light-hole–heavy-hole mixing, i.e., the mixing of the X and Y orbital states due to the C_{v2} symmetry of a (001) interface [19,29,51]. When the consideration is restricted to four valence bands, the interface mixing Hamiltonian of a single QW takes the following form [29]:

$$\hat{H}_{l-h} = t_{l-h}(\hbar^2/\sqrt{3}m_0 a_0)\{J_x, J_y\}_s \delta(z + L/2) - t_{l-h}(\hbar^2/\sqrt{3}m_0 a_0)\{J_x, J_y\}_s \delta(z - L/2). \quad (10)$$

Here t_{l-h} is the real dimensionless mixing parameter, and a_0 is the lattice constant. For the symmetric QW that we are concerned with in this study, the sign of t_{l-h} is irrelevant. $\hat{H}_{l-h}$ describes scattering processes where light holes turn into heavy holes (and vice versa) as they cross the interface plane. The explicit matrix form of $\{J_x, J_y\}_s$ is

$$\{J_x, J_y\}_s = \frac{1}{2}(J_x J_y + J_y J_x) = \frac{\sqrt{3}}{2}\begin{pmatrix} 0 & 0 & -i & 0 \\ 0 & 0 & 0 & -i \\ i & 0 & 0 & 0 \\ 0 & i & 0 & 0 \end{pmatrix}. \quad (11)$$

As $\hat{H}_{l-h}$ is proportional to Dirac δ-functions localized at the interfaces, the first derivative of the eigenfunctions $\chi(z)$ will experience a jump at $z = \pm L/2$. This would not be the case for $t_{l-h} = 0$, because m_{hh} and m_{lh} are assumed to be constant throughout the entire structure. We would like to mention that the appearance of the strong δ-perturbations at the interfaces is caused by the existence of a linear defect, which is a result of mismatching atomic bonds in the materials on the two sides of the interface plane. These δ-contributions lead to the interface mixing of the heavy-hole and light-hole states. The particular form of $\hat{H}_{l-h}$ used in our work was previously derived from the mixing between the X- and Y-atomic orbitals that is possible due to the C_{2v} symmetry of a (001) interface, which was proposed by Ivchenko *et al.* in

Ref. [29] and is widely used for the analysis of the interface light-hole–heavy-hole mixing. Since the interfaces reduce the translational and point symmetries of the system, they can lead not only to mixing between electronic states from the same band but also to intervalley and interband or intersubband mixing. In zinc-blende-based heterostructures grown along the [001] crystallographic axis, the lack of microscopic translational symmetry can result in remarkable coupling between Γ and X_z valley states as well as between the indirect X_x and X_y valley states.

B. Finite-difference method

We employ the finite-difference method to find a few of the highest eigenvalues of the effective envelope function Hamiltonian $\hat{H} = \hat{H}_L(z) + \hat{H}_Z + \hat{H}_{l-h}$. As we consider heavy-hole–light-hole interface mixing, we solve an eigenproblem for the envelope function $\chi(z)$, which is a z-dependent column vector with four elements. Two of these elements correspond to the heavy-hole states ($m_J = \pm 3/2$) and the other two describe the light holes ($m_J = \pm 1/2$). Since these states get mixed at the interfaces, the resulting eigenvectors may contain heavy-hole and light-hole elements with comparable magnitudes. The four-component envelope function $\chi(z)$ is discretized on a uniform z-grid $z_j = -\frac{W}{2} + j\Delta z$. The width of the grid $W = 5L$ and the grid step $\Delta z = L/500$ are chosen to adequately represent details of the envelope inside the QW, as well as its evanescent tails outside. The z-dependent operators entering $\hat{H}$ are replaced with their discrete versions according to the following symmetric rules:

$$\left.\frac{\partial^2 \chi}{\partial z^2}\right|_{z_j} \mapsto \frac{1}{(\Delta z)^2}[\chi(z_{j+1}) - 2\chi(z_j) + \chi(z_{j-1})], \tag{12}$$

$$\left\{z, -i\frac{\partial}{\partial z}\right\}_s \chi\Big|_{z_j} \mapsto \frac{1}{4i\Delta z}[(z_j + z_{j+1})\chi(z_{j+1}) - (z_j - z_{j+1})\chi(z_{j-1})], \tag{13}$$

$$\delta(z-a) \mapsto \begin{cases} \frac{1}{2\Delta z}, & z = a, \\ \frac{1}{4\Delta z}, & z = a \pm \Delta z, \\ 0 & \text{otherwise.} \end{cases} \tag{14}$$

With these discretization rules, $\hat{H}$ becomes a matrix of size $4N$, where N is the total number of grid points. Thanks to the local nature of the first and second derivative operators, this matrix has a block tridiagonal structure with each 4×4 block acting in m_J space.

We perform partial diagonalization of the resulting sparse matrix to find a few extremal eigenvalues using the implicitly restarted Lanczos method. The diagonalization procedure is implemented in C++ using the Eigen 3 matrix algebra library [52], the Arnoldi package (ARPACK) FORTRAN 77 library [53,54], and the EZARPACK C++ wrapper around it [55]. The hole Landé factors are computed from the difference of the two highest energy levels, $|g_h| = |E_0^h - E_1^h|/(\mu_B B)$. E_0^h and E_1^h are the two spin-split levels of the hole ground state.

V. DISCUSSION

Using the theoretical approach presented in Sec. IV, we calculate the dependence of the modified in-plane $|g_h|$ on the magnetic field strength for ZnSe- and CdTe-based QWs. The results for the ZnSe-based QWs are shown in Figs. 2(b) and 4(b). We use the following set of parameters for ZnSe: $\gamma_1 = 2.45$, $\gamma_2 = 0.61$, $\gamma_3 = 1.11$, and $\varepsilon_{\text{in}} - \varepsilon_{\text{out}} = 0.1$ eV [43]. Confinement energies of the light and heavy holes in the square-well potential without the interface mixing are estimated to be 12.7 meV/5.3 meV in sample no. 1, and 8.3 meV/3.3 meV in sample no. 2. The mixing parameter $t_{l-h} = 1.5$ is taken the same for samples no. 1 and no. 2, and the value of the mixing parameter was selected in such a way as to reproduce the experimentally measured behavior of $|g_h|$ in the best way. The calculations reproduce well the experimental data and reveal the same tendency for the increase of $|g_h|$ in stronger magnetic fields.

Calculations for the CdTe-based QW are performed for $\gamma_1 = 4.72$, $\gamma_2 = 1.29$, $\gamma_3 = 1.85$ [47], and $\varepsilon_{\text{in}} - \varepsilon_{\text{out}} = 0.106$ eV. The square-well confinement energies are 11.7 meV for the light holes and 4.2 meV for the heavy holes. The optimal correspondence between experimental data and theoretical calculations is achieved for the mixing parameter $t_{l-h} = 2.0$. The results are shown in Fig. 6.

To analyze the efficiency of the interface mixing of the heavy and light holes, we also calculate the dependence of the heavy-hole and light-hole probability densities [$|\chi_{\pm 3/2}(z)|^2$ and $|\chi_{\pm 1/2}(z)|^2$, respectively] on the coordinate z along the

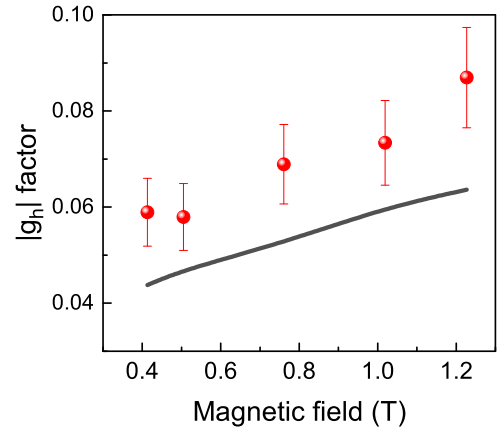

FIG. 6. 20-nm-thick CdTe/$Cd_{0.78}Mg_{0.22}$Te QW (sample no. 3). Magnetic field dependence of in-plane $|g_h|$: experimental data (red symbols) and calculated values (black line); for details, see Sec. IV B). $E_{\text{ex}} = 1.597$ eV, $P_{\text{pump}} = 4.2$ W/cm^2, $P_{\text{probe}} = 0.7$ W/cm^2, and $T = 1.7$ K.

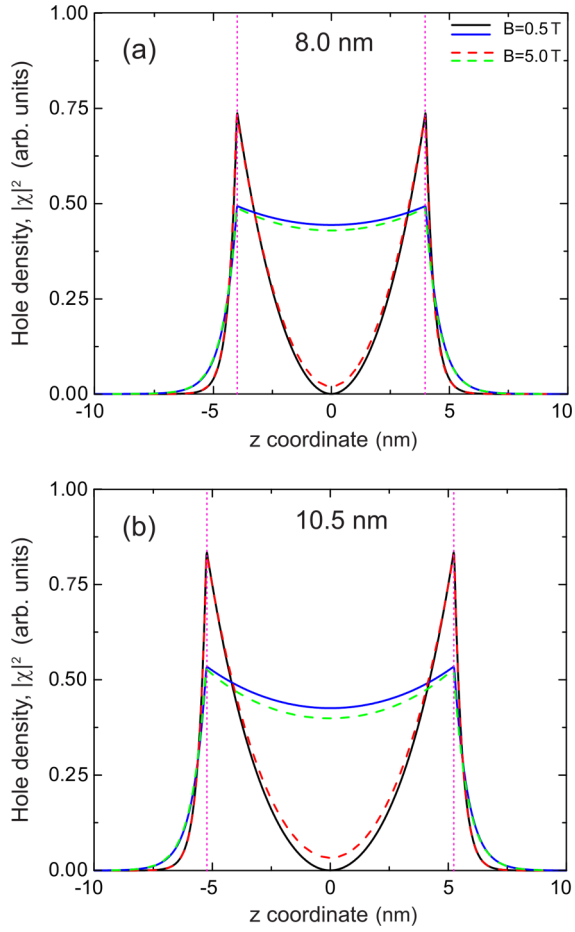

FIG. 7. Dependence of the heavy-hole and light-hole probability density in the ZnSe-based QWs corresponding to the highest valence-band energy level on the coordinate z along the QW growth axis (the coordinate of the QW center is the zero on the horizontal axis) for different values of the magnetic field. The solid lines correspond to $B = 0.5$ T and the dashed lines demonstrate the results calculated for $B = 5$ T. Panel (a) shows the calculations performed for sample no. 1 (QW width 8 nm) and panel (b) shows the results for sample no. 2 (QW width 10.5 nm). The solid black and dashed red lines depict the heavy-hole probability density $|\chi_{\pm 3/2}(z)|^2$; the solid blue and dashed green lines depict that of the light hole $|\chi_{\pm 1/2}(z)|^2$. The dashed vertical lines show the interfaces of the QWs.

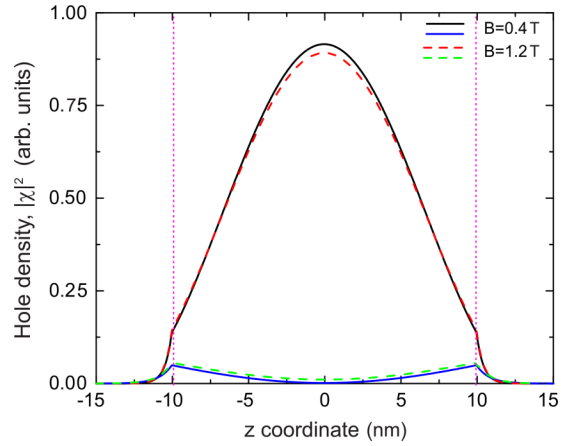

FIG. 8. Dependence of the heavy-hole and light-hole probability density in the 20-nm-thick CdTe-based QW corresponding to the highest valence-band energy level on the coordinate z along the QW growth axis (the coordinate of the QW center is the zero on the horizontal axis) for different values of the magnetic field. The solid lines correspond to a magnetic field of $B = 0.5$ T and the dashed lines demonstrate the results calculated for a magnetic field of $B = 5$ T. The solid black and dashed red lines depict the heavy-hole probability density $|\chi_{\pm 3/2}(z)|^2$; the solid blue and dashed green lines depict that of the light holes $|\chi_{\pm 1/2}(z)|^2$. The dashed vertical lines show the interfaces of the QWs.

QW growth axis for the energies corresponding to the highest valence-band energy level at different magnetic fields; see Fig. 7 for the ZnSe-based QW and Fig. 8 for the CdTe-based QW. One can see that the increase of the magnetic field only slightly modifies the densities of both heavy and light holes. It is worth noting that for the ZnSe-based QW, the δ-function mixing term confines heavy holes strongly at each heterointerface with the chosen values of t_{l-h}. The probability density for both light and heavy holes shows cusplike maxima at both interfaces and minima at the well centers (zero for the heavy holes and shallow minima for the light holes). For the ZnSe-based QW, the density of the heavy hole slightly increases and the density of the light hole decreases with increasing magnetic field. The opposite situation occurs in the CdTe-based QW. The most notable fact here is that in the ZnSe-based QWs, the interface mixing between heavy and light holes is much stronger than in the CdTe-based QW. For the ZnSe-based QWs, the probability densities of heavy and light holes have comparable amplitudes, while for the CdTe-based QW the density of the light holes is much smaller than the density of the heavy holes, despite the fact that in our modeling the mixing parameter for the CdTe-based QW is larger than that for the ZnSe-based QWs. In the wider CdTe-based QW, the square well confining potential for the heavy-hole states dominates the δ-function confinement leading to a heavy-hole probability density with a maximum corresponding to the center of the QW. The probability density associated with the light holes is still dominated by the δ functions at the interfaces. The peculiarities of the holes' spatial localization can be described by a combination of effective mass, depth, and width of the QW. It occurs that for heavy holes it is much more favorable to be localized in the wide QW, while for light holes localization at the interfaces is more effective. So heavy holes are not so strongly influenced by the interface mixing in the wide QW, while light holes reveal the behavior dominated by the confinement at the interfaces. The analysis of the interplay between QW confinement determined by the well parameters and the interface mixing will be given below (see Fig. 9).

The calculation results reveal different behaviors for the heavy-hole probability densities in the ZnSe-based QWs and the CdTe-based QW. This difference demonstrates a more pronounced role of the interface mixing in the ZnSe-based QWs in comparison with the CdTe-based QW. This is the direct consequence of two net effects. First, the CdTe-based QW is more than two times wider than the ZnSe-based QWs. So, the interface mixing of the heavy and light holes does not

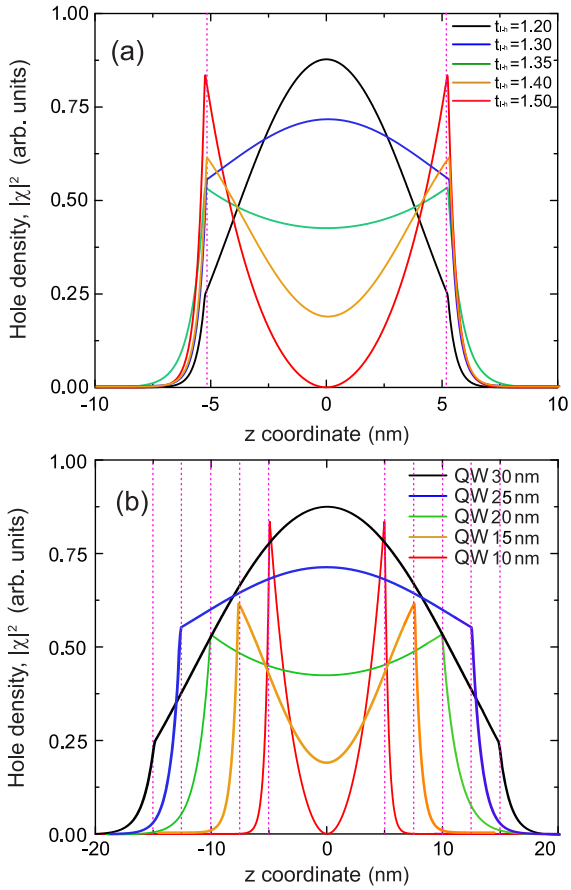

FIG. 9. Dependence of the heavy-hole probability density $|\chi_{\pm 3/2}(z)|^2$ in the ZnSe-based QWs corresponding to the highest valence-band energy level on the coordinate z along the QW growth axis (the coordinate of the center of the QW is the zero on the horizontal axis). Panel (a) shows the calculations for the 10.5 nm width QW for different values of the mixing parameter t_{l-h}. Panel (b) shows the results for different widths of the QW using the fixed value of the mixing parameter $t_{l-h} = 1.5$. All the curves are obtained for the external magnetic field $B = 0.5$ T. The dashed vertical lines show the interfaces of the QWs.

effect so much the density of states in the center of the QW, as is the case for the narrow ZnSe-based QWs. Second, the mixing parameters t_{l-h} are quite different for the ZnSe-based and CdTe-based QWs. The values of the mixing parameters are taken such that a good fit of the measured dependencies of $|g_h|$ on the magnetic field is obtained. In spite of the mixing parameter for CdTe-based QW being larger than for the ZnSe-based QWs, the interface mixing is weaker for the CdTe-based structure as the density of light-hole states is much smaller than the density of heavy-hole states, and the probability density for both heavy and light holes is not so strongly modified in the CdTe-based QW as it is in the ZnSe-based QW. A similar behavior of the heavy-hole probability density in both types of QWs can be achieved either by decreasing the width of the CdTe-based QW or by increasing the width of the ZnSe-based QWs. Numerically calculated results of the heavy-hole probability density in the QW for either changing the mixing parameter t_{l-h} value for fixed QW width or changing the QW width for fixed value of the mixing parameter t_{l-h} are shown in Fig. 9. Calculation results demonstrate directly the interplay between the QW confining potential and the interface mixing. It occurs that a critical value of both the QW width and the interface mixing is present in the system. For a fixed value of interface mixing, the hole probability distribution can be tuned by the QW width changing and vice versa. We would also like to mention that the presence of competition between the rectangular QW potential and the localizing complex "potential" at the interfaces makes the physical picture rather complicated. These two contributions have "incompatible" matrix structures. The interface mixing term localizes a mixture of the heavy and light holes as it has only off-diagonal matrix elements. By contrast, the quantum-well potential localizes the heavy and light holes independently and at different energies due to the different effective masses.

VI. CONCLUSIONS

We have measured experimentally and analyzed theoretically the magnetic field dependence of the in-plane hole g-factor value, $|g_h|$, in ZnSe- and CdTe-based QWs. The Zeeman effect and the interface mixing of heavy and light holes have been considered, and the interplay between these two effects has been analyzed. By comparing the experimental measurements with the calculation results, we found that the interface mixing is more pronounced for the narrow ZnSe-based QWs. The interface mixing only slightly modifies the heavy-hole probability density in the wide CdTe-based QW, where the Zeeman effect plays the main role in the modification of the hole g factor.

ACKNOWLEDGMENTS

The authors are thankful to M. M. Glazov and M. V. Durnev for fruitful discussions. We acknowledge the financial support by the Deutsche Forschungsgemeinschaft in the frame of the International Collaborative Research Center TRR 160 (Project A1). V.N.M. acknowledges the support of the Russian Science Foundation (Grant No. 18-72-10002–theoretical calculations). The research in Poland was partially supported by the Foundation for Polish Science through the IRA Programme cofinanced by EU within SG OP (Grant No. MAB/2017/1) and by the National Science Centre through Grants No. 2017/25/B/ST3/02966 and No. 2018/30/M/ST3/00276.

[1] *Spin Physics in Semiconductors*, edited by M. I. Dyakonov (Springer International AG, Berlin, 2017).

[2] *Semiconductor Spintronics and Quantum Computation*, edited by D. D. Awschalom, D. Loss, and N. Samarth (Springer, Berlin, 2002).

[3] E. L. Ivchenko, *Optical Spectroscopy of Semiconductor Nanostructures* (Alpha Science International, Harrow, UK, 2005).

[4] E. A. Zhukov, V. N. Mantsevich, D. R. Yakovlev, N. E. Kopteva, E. Kirstein, A. Waag, G. Karczewski, T. Wojtowicz, and M.

Bayer, Renormalization of the electron g factor in the degenerate two-dimensional electron gas of ZnSe- and CdTe-based quantum wells, Phys. Rev. B **102**, 125306 (2020).

[5] E. A. Zhukov, D. R. Yakovlev, M. Gerbracht, G. V. Mikhailov, G. Karczewski, T. Wojtowicz, J. Kossut, and M. Bayer, Spin coherence of holes and electrons in undoped CdTe/(Cd, Mg)Te quantum wells, Phys. Rev. B **79**, 155318 (2009).

[6] M. Kugler, T. Andlauer, T. Korn, A. Wagner, S. Fehringer, R. Schulz, M. Kubová, C. Gerl, D. Schuh, W. Wegscheider, P. Vogl, and C. Schüller, Gate control of low-temperature spin dynamics in two-dimensional hole systems, Phys. Rev. B **80**, 035325 (2009).

[7] M. Kugler, K. Korzekwa, P. Machnikowski, C. Gradl, S. Furthmeier, M. Griesbeck, M. Hirmer, D. Schuh, W. Wegscheider, T. Kuhn, C. Schüller, and T. Korn, Decoherence-assisted initialization of a resident hole spin polarization in a p-doped semiconductor quantum well, Phys. Rev. B **84**, 085327 (2011).

[8] M. Syperek, D. R. Yakovlev, A. Greilich, J. Misiewicz, M. Bayer, D. Reuter, and A. D. Wieck, Spin coherence of holes in GaAs/(Al, Ga)As quantum wells, Phys. Rev. Lett. **99**, 187401 (2007).

[9] B. D. Gerardot, D. Brunner, P. A. Dalgarno, P. Öhberg, S. Seidl, M. Kroner, K. Karrai, N. G. Stoltz, P. M. Petroff, and R. J. Warburton, Optical pumping of a single hole spin in a quantum dot, Nature (London) **451**, 441 (2008).

[10] T. Korn, M. Kugler, M. Griesbeck, R. Schulz, A. Wagner, M. Hirmer, C. Gerl, D. Schuh, W. Wegscheider, and C. Schüller, Engineering ultralong spin coherence in two-dimensional hole systems at low temperatures, New J. Phys. **12**, 043003 (2010).

[11] B. Eble, C. Testelin, P. Desfonds, F. Bernardot, A. Balocchi, T. Amand, A. Miard, A. Lemaître, X. Marie, and M. Chamarro, Hole–Nuclear Spin Interaction in Quantum Dots, Phys. Rev. Lett. **102**, 146601 (2009).

[12] E. A. Chekhovich, A. B. Krysa, M. S. Skolnick, and A. I. Tartakovskii, Direct Measurement of the Hole-Nuclear Spin Interaction in Single InP/GaInP Quantum Dots Using Photoluminescence Spectroscopy, Phys. Rev. Lett. **106**, 027402 (2011)

[13] E. A. Chekhovich, M. M. Glazov, A. B. Krysa, M. Hopkinson, P. Senellart, A. Lemaître, M. S. Skolnick, and A. I. Tartakovskii, Element-sensitive measurement of the hole–nuclear spin interaction in quantum dots, Nat. Phys. **9**, 74 (2013).

[14] J. Puls, M. Rabe, A. Siarkos, and F. Henneberger, Excitonic properties of ZnSe/(Zn, Mg)Se quantum wells: A model study of the tensile-strain situation, Phys. Rev. B **57**, 14749 (1998).

[15] A. V. Koudinov, I. A. Akimov, Y. G. Kusrayev, and F. Henneberger, Optical and magnetic anisotropies of the hole states in Stranski-Krastanov quantum dots, Phys. Rev. B **70**, 241305(R) (2004).

[16] D. N. Krizhanovskii, A. Ebbens, A. I. Tartakovskii, F. Pulizzi, T. Wright, M. S. Skolnick, and M. Hopkinson, Individual neutral and charged $In_xGa_{1-x}As$-GaAs quantum dots with strong in-plane optical anisotropy, Phys. Rev. B **72**, 161312(R) (2005).

[17] M. Atatüre, J. Dreiser, A. Badolato, A. Högele, K. Karrai, and A. Imamoglu1, Quantum-dots-state preparation with near-unity fidelity, Science **312**, 551 (2006).

[18] C. Tonin, R. Hostein, V. Voliotis, R. Grousson, A. Lemaitre, and A. Martinez, Polarization properties of excitonic qubits in single self-assembled quantum dots, Phys. Rev. B **85**, 155303 (2012).

[19] M. V. Durnev, Zeeman splitting of lighthole in quantum wells: Comparison of theory and experiments, Phys. Solid State, **56**, 1416 (2014) [Fiz. Tverd. Tela, **56**, 1364 (2014)].

[20] T. Belhadj, T. Amand, A. Kunold, C.-M. Simon, T. Kuroda, M. Abbarchi, T. Mano, K. Sakoda, S. Kunz, X. Marie, and B. Urbaszek, Impact of heavy hole-light hole coupling on optical selection rules in GaAs quantum dots, Appl. Phys. Lett. **97**, 051111 (2010).

[21] S. Ohno, S. Adachi, R. Kaji, S. Muto, and H. Sasakura, Optical anisotropy and photoluminescence polarization in single InAlAs quantum dots, Appl. Phys. Lett. **98**, 161912 (2011).

[22] F. Fras, F. Bernardot, B. Eble, M. Bernard, B. Siarry, A. Miard, A. Lemaître, C. Testelin, and M. Chamarro, The role of heavy–light-hole mixing on the optical initialization of hole spin in InAs quantum dots, J. Phys.: Condens. Matter **25**, 202202 (2013).

[23] E. W. Bauer and T. Ando, Exciton mixing in quantum wells, Phys. Rev. B **38**, 6015 (1988).

[24] C. Y.-P. Chao and S. L. Chuang, Momentum-space solution of exciton excited states and heavy-hole–light-hole mixing in quantum wells, Phys. Rev. B **48**, 8210 (1993).

[25] S. Nojima, Anisotropy of optical transitions in (110)-oriented quantum wells, Phys. Rev. B **47**, 13535 (1993).

[26] E. L. Ivchenko, A. Yu. Kaminski, and I. L. Aleiner, Exchange splitting of excitonic levels in types I and II superlattices, JETP **77**, 609 (1993).

[27] G. Edwards and J. C. Inkson, Hole states in GaAs/AlAs heterostructures and the limitations of the Luttinger model, Solid State Commun. **89**, 595 (1994).

[28] Y.-C. Chang and J. N. Schulman, Interband optical transitions in GaAs-$Ga_{1-x}Al_xAs$ and InAs-GaSb superlattices, Phys. Rev. B **31**, 2069 (1985).

[29] E. L. Ivchenko, A. Yu. Kaminski, and U. Rössler, Heavy-light hole mixing at zinc-blende (001) interfaces under normal incidence, Phys. Rev. B **54**, 5852 (1996).

[30] A. Arora, A. Mandal, S. Chakrabarti, and S. Ghosh, Magneto-optical Kerr effect spectroscopy based study of Landé g-factor for holes in GaAs/AlGaAs single quantum wells under low magnetic field, J. Appl. Phys. **113**, 213505 (2013).

[31] N. Ares, V. N. Golovach, G. Katsaros, M. Stoffel, F. Fournel, L. I. Glazman, O. G. Schmidt, and S. De Franceschi, Nature of Tunable Hole g Factors in Quantum Dots, Phys. Rev. Lett. **110**, 046602 (2013).

[32] J. H. Prechtel, F. Maier, J. Houel, A. V. Kuhlmann, A. Ludwig, A. D. Wieck, D. Loss, and R. J. Warburton, Electrically tunable hole g factor of an optically active quantum dot for fast spin rotations, Phys. Rev. B **91**, 165304 (2015).

[33] G. Bartsch, M. Gerbracht, D. R. Yakovlev, J. H. Blokland, P. C. M. Christianen, E. A. Zhukov, A. B. Dzyubenko, G. Karczewski, T. Wojtowicz, J. Kossut, J. C. Maan, and M. Bayer, Positively versus negatively charged excitons: A high magnetic field study of CdTe/$Cd_{1-x}Mg_x$Te quantum wells, Phys. Rev. B **83**, 235317 (2011).

[34] E. V. Shornikova, L. Biadala, D. R. Yakovlev, D. Feng, V. F. Sapega, N. Flipo, A. A. Golovatenko, M. A. Semina, A. V. Rodina, A. A. Mitioglu, M. V. Ballottin, P. C. M. Christianen, Y. G. Kusrayev, M. Nasilowski, B. Dubertret, and M. Bayer, Electron and hole g-Factors and spin dynamics of negatively charged excitons in CdSe/CdS colloidal nanoplatelets with thick shells, Nano Lett. **18**, 373 (2018).

[35] E. A. Zhukov, D. R. Yakovlev, A. Schwan, O. A. Yugov, A. Waag, L. W. Molenkamp, and M. Bayer, Spin coherence of electrons and holes in ZnSe-based quantum wells studied by pump-probe Kerr rotation, Phys. Status Solidi B **251**, 1872 (2014).

[36] G. V. Astakhov, D. R. Yakovlev, V. P. Kochereshko, W. Ossau, J. Nürnberger, W. Faschinger, and G. Landwehr, Charged excitons in ZnSe-based quantum wells, Phys. Rev. B **60**, R8485(R) (1999).

[37] G. V. Astakhov, V. P. Kochereshko, D. R. Yakovlev, W. Ossau, J. Nürnberger, W. Faschinger, and G. Landwehr, Oscillator strength of trion states in ZnSe-based quantum wells, Phys. Rev. B **62**, 10345 (2000).

[38] G. V. Astakhov, V. P. Kochereshko, D. R. Yakovlev, W. Ossau, J. Nürnberger, W. Faschinger, G. Landwehr, T. Wojtowicz, G. Karczewski, and J. Kossut, Optical method for the determination of carrier density in modulation-doped quantum wells, Phys. Rev. B **65**, 115310 (2002).

[39] G. V. Astakhov, D. R. Yakovlev, V. P. Kochereshko, W. Ossau, W. Faschinger, J. Puls, F. Henneberger, S. A. Crooker, Q. McCulloch, D. Wolverson, N. A. Gippius, and A. Waag, Binding energy of charged excitons in ZnSe-based quantum wells, Phys. Rev. B **65**, 165335 (2002).

[40] W. Maśana, P. Kossacki, M. Bertolini, H. Boukari, D. Ferrand, S. Tatarenko, J. Cibert, and J. A. Gaj, *p*-type doping of II–VI heterostructures from surface states: Application to ferromagnetic $Cd_{1-x}Mn_xTe$ quantum wells, Appl. Phys. Lett. **82**, 1875 (2003).

[41] W. Maśana, Ferromagnétism induit par les porteurs dans des puits quantiques de (Cd,Mn)Te: Etude spectroscopique du desordre, doctoral thesis, L'Úniversite Joseph Fourier, 2007.

[42] D. R. Yakovlev and M. Bayer, in *Spin Physics in Semiconductors*, 2nd ed., edited by M. I. Dyakonov (Springer International AG, Berlin, 2017), Chap. 6, p. 155.

[43] Landolt-Börnstein, Group III, Condensed Matter, *Semiconductors: II-VI and I-VII Compounds; Semimagnetic Compounds*, edited by O. Madelung, U. Rössler, and M. Schulz (Springer, Berlin, 1999), Vol. III.41.B.

[44] M. Yu. Petrov, I. V. Ignatiev, S. V. Poltavtsev, A. Greilich, A. Bauschulte, D. R. Yakovlev, and M. Bayer, Effect of thermal annealing on the hyperfine interaction in InAs/GaAs quantum dots, Phys. Rev. B **78**, 045315 (2008).

[45] A. Greilich, A. Pawlis, F. Liu, O. A. Yugov, D. R. Yakovlev, K. Lischka, Y. Yamamoto, and M. Bayer Spin dephasing of fluorine-bound electrons in ZnSe, Phys. Rev. B **85**, 121303(R) (2012).

[46] G. Bastard, *Wave Mechanics Applied to Semiconductor Heterostructures, Monographies de Physique* (Les Ulis Cedex, France, 1988).

[47] G. Milchber, K. Saminadayar, E. Molva, H. R. Zelsmann, Properties of nitrogen acceptor in CdTe: Energy spectrum and interaction with hydrogen, Phys. Status Solidi B **125**, 795 (1984).

[48] B. Venitucci and Y.-M. Niquet, Simple model for electrical hole spin manipulation in semiconductor quantum dots: Impact of dot material and orientation, Phys. Rev. B **99**, 115317 (2019).

[49] J. M. Luttinger, Quantum theory of cyclotron resonance in semiconductors: General theory, Phys. Rev. **102**, 1030 (1956).

[50] L. M. Roth, Theory of the faraday effect in solids, Phys. Rev. **133**, A542 (1964).

[51] I. L. Aleiner and E. L. Ivchenko, Anisotropic exchange splitting in type II GaAs/AlAs superlattices, Pis'ma Zh. Eksp. Teor. Fiz. **55**, 662 (1992) [JETP Lett. **55**, 692 (1992)].

[52] G. Guennebaud, B. Jacob *et al.*, Eigen v3. http://eigen.tuxfamily.org (2020).

[53] R. B. Lehoucq, D. C. Sorensen, and C. Yang, *ARPACK Users' Guide: Solution of Large-scale Eigenvalue Problems with Implicitly Restarted Arnoldi Methods* (SIAM, Philadelphia, 1998).

[54] ARPACK-NG, Collection of Fortran77 subroutines designed to solve large scale eigenvalue problems. https://github.com/opencollab/arpack-ng.

[55] I. Krivenko, ezARPACK—A C++ ARPACK-NG wrapper compatible with multiple matrix/vector algebra libraries: Release 0.9. Zenodo (July, 2020).